



DETERMINING PLASTIC HINGE LENGTH OF HIGH PERFORMANCE RC BEAMS

Y. Sumer⁽¹⁾

⁽¹⁾ Associate Prof., Sakarya University, Technology Faculty, ysumer@sakarya.edu.tr

Abstract

During earthquake concrete structures dissipate energy by deforming inelastically. The plastic deformation localized in a small zone namely the plastic hinge zone is critical for flexural members as it governs the load carrying and deformation capacities of the member. Pushover analysis, one method of nonlinear static analysis, is generally used in the assessment of existing buildings. Pushover analysis gives more realistic results when compared to linear analysis methods to achieve seismic performance level of structures. In pushover analysis nonlinear hinge properties of each member should be addressed. The formation of a plastic hinge in structural member depends on both the dynamic characteristic of earthquake and structural member properties such as dimension and material properties. Because of the difficulty and high complexity included, the behavior of plastic hinge of reinforced concrete flexural members has been previously investigated experimentally. Due to the high non-linearity occurs in plastic hinge zone and restrictions by the time and cost especially in large tests, very limited knowledge has been obtained up to date. Moreover past studies showed that none of the existing empirical models is adequate for prediction of plastic hinge length. This study tries to investigate the problem numerically using Nonlinear Finite Element Modeling (FEM) approach by employing software package ABAQUS. To achieve this, a numerical model is generated and verified with existing experimental studies obtained from the literature, by comparing load deflection response and rotational capacity of the test elements. Parametric studies are performed to investigate the plastic hinge length in terms of material properties concrete and dimensions of the member. High performance concrete is selected to be as C50, C60 and C80. With the calibrated FEM model, the extent of the rebar yielding zone and concrete crush zone are examined to define the plastic hinge length.

Keywords: high performance concrete; plastic hinge length; finite element analysis



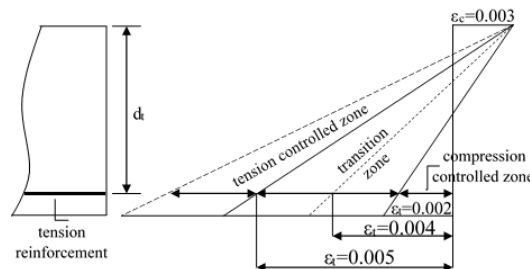
1. Introduction

Energy dissipation of reinforced concrete (RC) structures can be determined numerically by applying full-range analysis beyond plastic phase. In this analysis, yielding of reinforcement and crushing of concrete can be seen over a finite region known as plastic hinge length where the critical moment is present. Plastic hinge region of RC flexural members is a critical zone need to be given intensive care to prevent failure of structural members from extreme events such as earthquakes. There is no adequate determination of plastic hinge length of concrete structural elements. However, the length of plastic hinge region, L_p , is defined as the length over which the longitudinal reinforcement yields [1]. The performance of a plastic hinge is crucial to the load carrying and deformation capacities of flexural members of structures. The accuracy of the results obtained from nonlinear analysis is also directly related to the hinge definitions of the structure. Thus, plastic hinge length of RC members has been an interesting and complicated subject for researchers.

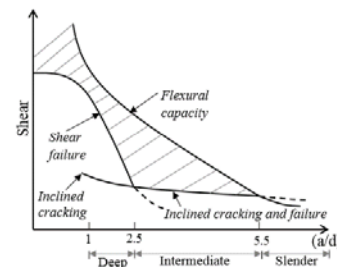
There is no definitive theoretical formulations to calculate plastic hinge length in the literature. Present calculations are based on empirical equations observed from tests [2-6]. Park and Paulay found that plastic hinge length of beams under monotonic loading is affected by concrete compressive strength, concrete ultimate strain, shear-span to depth ratio, and effective depth of section [7]. Mechanical properties of steel also affect L_p . Beeby studied the effects of the ratio of ultimate strength to yield strength of longitudinal reinforcement, f_u/f_y , and the ultimate strain, ϵ_u on plastic hinge length [8]. Several expressions have been proposed for determining the equivalent plastic hinge length of beams and columns; some of these equations (Eq. 1-5) are summarized as follows;

Corley, (1966), [2]	$L_p = 0.5d + 0.2\sqrt{d}\left(\frac{z}{d}\right)$	(1)
Mattock, (1967), [3]	$L_p = 0.5d + 0.05z$	(2)
Paulay and Priestley, (1992), [4]	$L_p = 0.08z + 0.022d_b f_y \geq 0.044d_b f_y$	(3)
Panagiotakos and Fardis, (2001), [5]	$L_p = 0.18z + 0.021d_b f_y$	(4)
Fema 356, (2000), [6]	$L_p = 0.5d$	(5)

In these equations, L_p is the plastic hinge length, d is effective depth of the beam, z is the critical distance from the critical section to the point of contraflexure, and f_y and d_b are the expected yield strength and the diameter of longitudinal reinforcement, respectively. There are some recent studies, which defines L_p for columns [9-12]. Since the axial load level is included in those expression they are not considered here in this study. Limit state failure in flexure is achieved when continues increases in the external load reaches the capacity of the beam. If the designer proportion the beam to allow concrete and steel reach their capacity prior to failure, both materials will fail simultaneously at the limit state. Moreover, compression failure of concrete before the tension failure of steel should be avoided to confirm an adequate rotation capacity at limit state. This reserved rotation capacity will prevent brittle failure in case of overload or will cope with additional tensile forces created from different settlement of foundations, creep and shrinkage of concrete. Strain of tension reinforcement will be the determinant variable that defines the type of failure; tension controlled (ductile type of failure), compression controlled (brittle type of failure) and between. Thus, the amount of the tension reinforcement will determine the amount of strain and failure type of the beam. This behavior according to ACI 318-14 is illustrated in Fig. 1a.



a) failure type of beams regarding to tensile strain of reinforcement, [13]



b) determination of beam slenderness, [14]

Fig. 1 - Limit states of reinforced beam

The behavior of beam is also determined by the slenderness of the beam (Fig. 1b). Slenderness of RC beam is defined as the ratio of its shear span (a) to its depth (d). Deep beam with a/d from 1 to 2.5 will form few small cracks at mid-span but after the redistribution of internal forces bond failure between the tension reinforcement and surrounding concrete at support region follows. This is also known as shear compression failure. Intermediate beam with a/d from 2.5 to 5.5 will fail at the inclined cracking load. Slender beam with a/d greater than about 5.5 will fail in flexure prior to the formation of inclined cracks giving sufficient warning of the collapse of the beam.

In this paper, determination of L_p considering yielding zone of tension reinforcement is investigated for beams designed to achieve different types of failures. Verified nonlinear finite element approach is employed in the research to minimize time and cost for large test specimens. With the verified numerical model, the extent of reinforcement yielding zone to address the plastic hinge length is studied for RC beams with various failure modes.

2. Development of Numerical Modeling

Finite element analysis has been widely used in civil engineering applications from steel structure analysis to RC analysis. [15-16]. Nonlinear finite element software package, ABAQUS is employed to simulate experimental testing. Numerical model is verified with existing experimental data obtained from literature especially for load-deflection relation and axial force distribution of tensile steel reinforcement. The latter verification is more important since determination of L_p in this study is made according to the yielding zone of tensile steel. Sensitivity of the numerical model against mesh density, dilation angle and fracture energy of concrete is also investigated.

Numerical model of simply supported beam under four-point loading is selected for verification purpose because it is the one obtained for both load-deflection relation and axial force distribution are studied with three dimensional model using 3d continuum elements and 3d truss elements for concrete and steel reinforcement, respectively. Shear dominant members are not modeled as individual finite members but their effects are included in concrete model by introducing confined concrete model. All the beams are loaded by displacement control in the vertical direction. Steel bars are merged into concrete elements by constraining the same degree of freedom at intersection joints of concrete and steel. This is achieved by embedding steel elements into concrete elements. (Fig. 2)

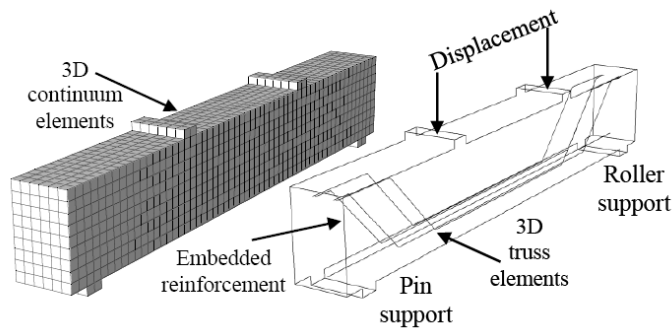


Fig. 2 - General layout of the beam used in numerical modeling

2.1. Nonlinear behavior of materials

Since the compression and tension stress-strain relation of the used materials are not reported in the test reports these relations are considered by using mathematical models from literature. Stress-strain curve of concrete under uniaxial compression is obtained by employing Hognestad parabola along with linear descending branch. Some modifications are made to this parabola according to CEB-FIP MC90 due to the effects of closed stirrups to catch the behavior of confined concrete [17].

Fig. 3a displays a schematic representation of the uniaxial material response. In the figure, σ is the compressive stress, f_{cu} is the ultimate compressive stress, ϵ_c^* is the peak compressive strain, E is the elastic modulus and f_c^* is the modified compressive strength. Bilinear model is adopted for tensile behavior of concrete as plotted in Fig. 3b [18]. Crack opening, calculated as a ratio of the total external energy supply per unit area required to create a crack, is used to define the tensile behavior. Tensile fracture energy of concrete, (G_F), is determined as a function of concrete compressive strength, f_c^* , and a coefficient, G_{fo} , which is related to the maximum aggregate size [19]. Yield surface of concrete considering both tension and compression is given in Fig. 3c. The effective cohesion stresses determine the size of the yield (or failure) surface [20]. The evolution of the yield surface is controlled by tensile and compressive equivalent plastic strains. Yield surface is defined by introducing four parameters; dilation angle (ψ) is measured in the p-q plane (p: hydrostatic pressure stress, which is a function of the first stress invariant, q : second deviatoric stress invariant) at high confining pressure. ϵ , is an eccentricity of the plastic potential surface with default value of 0.1. The ratio of initial biaxial compressive yield stress to initial uniaxial compressive yield stress is defined by σ_{bo}/σ_{co} , with a default value of 1.16. Finally, K_c is the ratio of the second stress invariant on the tensile meridian to compressive meridian at initial yield with default value of 2/3 [21].

This paper does not discuss the identification procedure for parameters; ϵ , σ_{bo}/σ_{co} , and K_c because tests that are going to be verified in this study do not have such information thus, default values are accepted. But dilation angle is an effective parameter for the numerical analysis and needs to be searched carefully in every model.

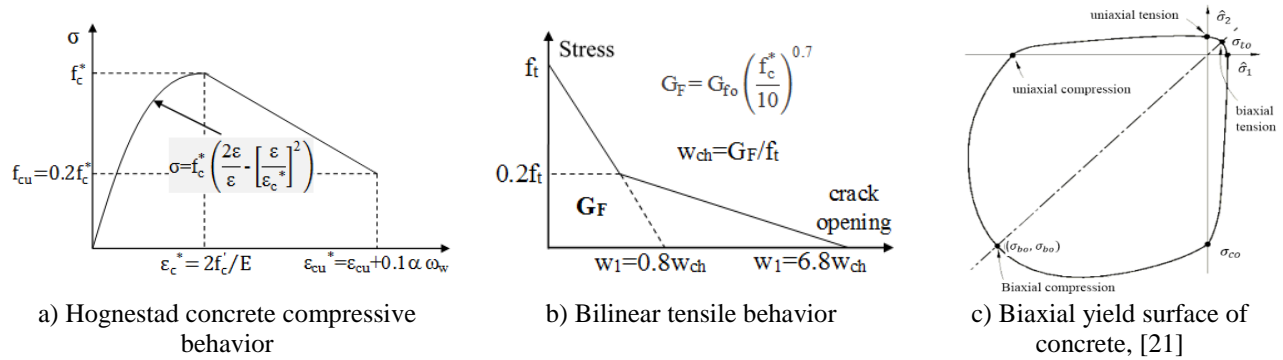


Fig. 3 - Material models and yield surface of concrete

Concrete Damaged Plasticity (CDP) model combining the effect of both damage and plasticity is used in this study. For CDP two main failure mechanisms are tensile cracking and compressive crushing of the concrete. The unloaded response of concrete is weakened due to the damages and degradation in the elastic stiffness of the material. Tensile and compressive response of concrete including damage parameter is given in Fig. 4. The degradation of the elastic stiffness on the stress-strain curve is characterized by two damage variables which can take values from zero to one for tension and compression as d_t and d_c , respectively. Zero represents the undamaged material where one represents total loss of strength [21]. E_o is the initial (undamaged) elastic stiffness of the material and $\tilde{\epsilon}_c^{pl}$, $\tilde{\epsilon}_t^{pl}$, $\tilde{\epsilon}_c^{in}$, $\tilde{\epsilon}_t^{ck}$ are compressive plastic strain, tensile plastic strain, compressive inelastic strain and tensile cracking strain respectively (Fig 4a). Thus final stress-strain relations considering degradation under uniaxial tension and compression are taken into account with Eq. (6) and Eq. (7).

In this study damage variable in compression is calculated by using the equations given in Fig. 4a [22]. The parameter b_c represents the relation between plastic and inelastic strains and can be determined using curve-fitting of cyclic tests [23]. Damage variable in tension is determined from bilinear behavior of concrete and values are plotted in Fig. 4b. Interface behavior between rebar and concrete is modeled by implementing tension stiffening effect into the concrete.

$$\sigma_t = (1-d_t) \cdot E_o \cdot (\epsilon_t - \tilde{\epsilon}_t^{pl}) \quad (6)$$

$$\sigma_c = (1-d_c) \cdot E_0 \cdot (\epsilon_c - \epsilon_c^{pl}) \tag{7}$$

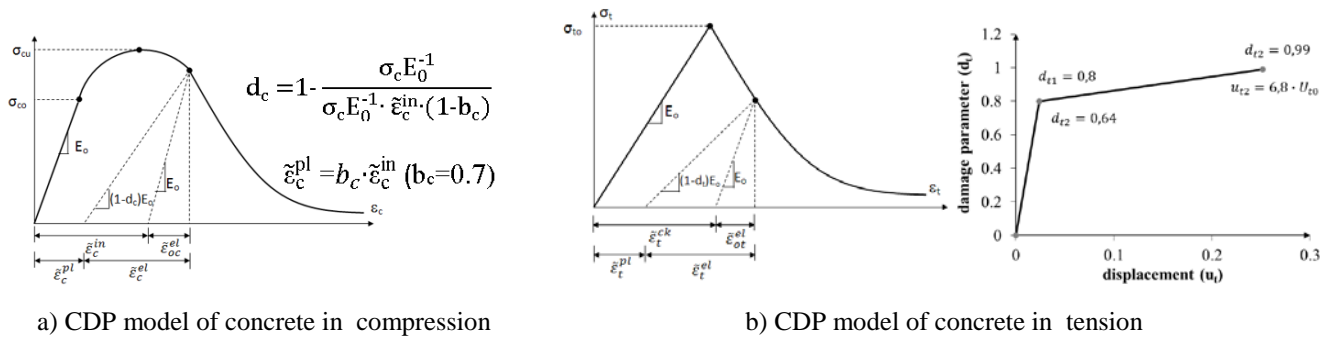


Fig. 4 - Concrete damage plasticity model [21]

Experimentally determined mechanical response values from coupon testing appear in Fig. 5 converted to an idealized multi-linear true stress and logarithmic strain format using the given equations.

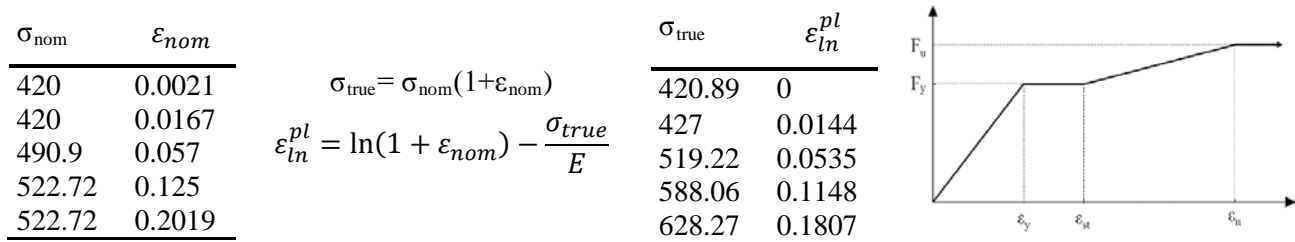
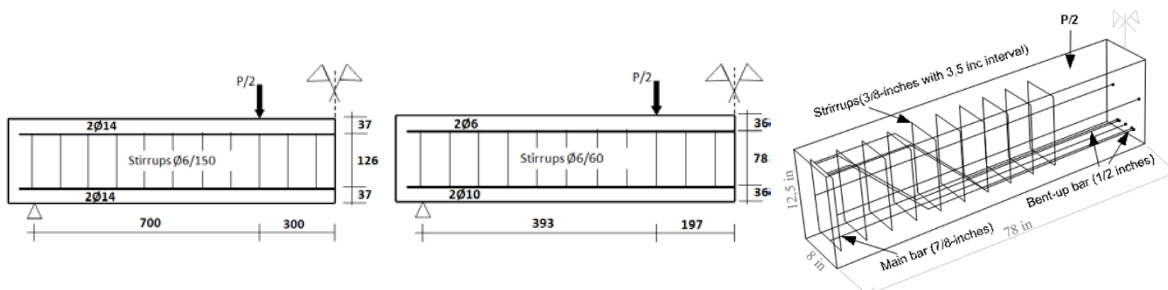


Fig. 5 - Material model for reinforcement steel, [24]

3. Numerical Model Verification

Since determination of yielding zone of reinforcement steel is at the heart of this study the ability of numerical model addressing the yielding zone of reinforcement steel must be verified with the existing test results so that further parametric studies can be made with the proposed numerical model. However, measuring the state of stress at the reinforcement is rather difficult due the surrounding concrete. Thus, very limited data is available at the literature. To have satisfying verification, test specimens constructed with a technique of installing strain gages through the center of the reinforcement by Mainst,1952 is selected for this study. Herein it is called Test case 3 and it is used to verify the ability of the numerical model to simulate the yielding of tensile reinforcement of RC beam.

Load-displacement relation is also important data to check whether the proposed model identify the rigidity of the experimental test specimen. Three experiments are selected for verification purposes. Test case 1 and 2 are used to show the robustness of the model to simulate the load-deflection relationship. Details of these two experiments can be found from Arduini et al., 1997, Sharif et al., 1994, respectively. Finally, Layout of experimental specimens are plotted in Fig. 6 and material properties are listed in Table 1.



Test case-1 [25]

Test case-2 [26]

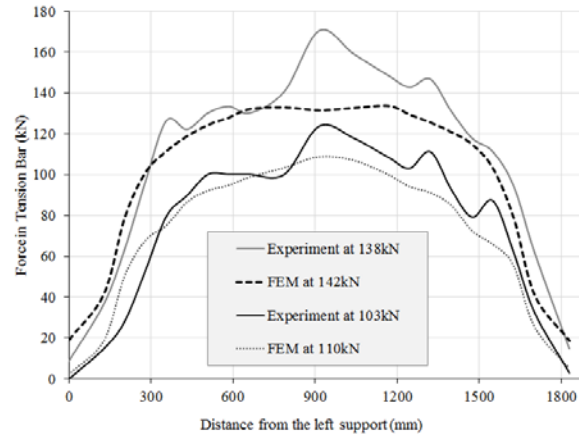
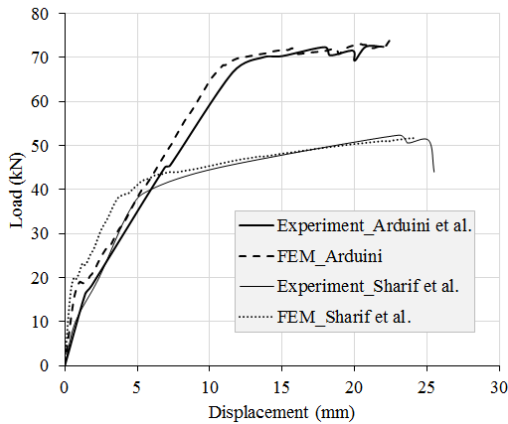
Test case-3 [27]

Fig. 6 - Layout of test beam (dimensions are mm in Test case-1 and 2)

When the verification results given in Fig. 7a are examined, it is concluded that proposed numerical modeling approach can successfully represent the experimental results. The stress distribution at tensile steel (main bar) for different load levels are compared from both experiment and numerical model in Fig. 7b. The difference where stress vary rapidly is believed to be the result of crack propagation which is not considered in numerical model. Other than that overall pattern of the diagrams agrees well.

Table 1 - Material properties of test beams.

Test Case	Beam Ref.No	E_c (GPa)	f_c (MPa)	f_t (MPa)	E_s (GPa)	f_y (MPa)	Tension Bars (mm)	Bent-up bars (mm)
1	A1	25	33	2.6	200	540	2Φ14	-
2	P1	27	37.7	-	200	450	2Φ10	-
3	B15	26.8	28.8	2.84	213.7	594.3	1x22.2	4x12.72



a) Load-deflection relationship obtained by using 35° and 30° dilation angle, 50 and 25mm mesh size and 16-8 mm aggregate size respectively.

b) Stresses at tension reinforcement of RC beam obtained by using 30° dilation angle, 35mm mesh and 16 mm aggregate size

Fig. 7 - Numerical model verification results

All these plots show that finite element modeling techniques applied herein, are valid for RC beams. Load deflection relation and stress distributions of individual element could be monitored very well. Based on these results, it appears that the present modeling techniques are sufficiently robust to undertake the further parametric study to investigate the effects of different parameters on plastic hinge regions of existing RC beams. Therefore performance of a plastic hinge and load carrying and deformation capacities of flexural members will be determined easily by the numerical studies.

4. Parametric Study

A parametric study using the aforesaid finite element modelling techniques was carried out to investigate the effect of tensile yielding on the L_p of reinforced concrete beams designed to achieve different failure mode (Table 2). Half of the beam is modeled with three different lengths to consider the slenderness effect and with three different tension reinforcement steel ratio to consider the ductile behavior. The nomination S , I and D represents the slenderness of beam stating, Slender, Intermediate and Deep as described according to Fig 1. All the beams are designed with steel ratio to be in transition zone with a value of $\epsilon_t=0.004$.



Table 2 - Parametric study for numerical beams to achieve different flexural behavior

		Slenderness		
		Deep (D)	Intermediate (I)	Slender (S)
Concrete Class	C50	Beam C50D	Beam C50I	Beam C50S
	C60	Beam C60D	Beam C60I	Beam C60S
	C80	Beam C80D	Beam C80I	Beam C80S

Geometry and material properties of test beams are presented in Table 3. The beams are loaded by displacement control until they fail. The length of loading span is taken as equal to the shear span, a . So the total length of the beam is $3a$. For the credence of the study, beams reinforcement scheme is applied identical with the Test case-3 used in the verification study.

Table 3 - Mechanical and geometrical variables of numerical beams used in parametric studies.

Specimen Name	ϵ_t (strain of steel)	ρ (reinforcement ratio)	a , mm	L , mm	a/d	L/h	f_c , MPa	f_t , MPa	E_c , GPa	f_y , MPa	E_s , GPa
C50S	$\epsilon_t=0.004$	0.0184	2000	6200	5.7	15.5	50	4.24	33.2	420	210
C60S	$\epsilon_t=0.004$	0.0184	2000	6200	5.7	15.5	60	4.65	36.4	420	210
C80S	$\epsilon_t=0.004$	0.0184	2000	6200	5.7	15.5	80	5.36	42.0	420	210
C50I	$\epsilon_t=0.004$	0.0184	1400	4500	4	11.25	50	4.24	33.2	420	210
C60I	$\epsilon_t=0.004$	0.0184	1400	4500	4	11.25	60	4.65	36.4	420	210
C80I	$\epsilon_t=0.004$	0.0184	1400	4500	4	11.25	80	5.36	42.0	420	210
C50D	$\epsilon_t=0.004$	0.0184	700	2400	2	6	50	4.24	33.2	420	210
C60D	$\epsilon_t=0.004$	0.0184	700	2400	2	6	60	4.65	36.4	420	210
C80D	$\epsilon_t=0.004$	0.0184	700	2400	2	6	80	5.36	42.0	420	210

5. Results and Discussions

Once the analysis is completed stress level at tension bar is investigated closely. Initiation and propagation of yielding for each loading step is checked until ultimate load point is reached. Stress level of tension bar is plotted at ultimate load level to determine the yielding zone of reinforcement. Moreover, cracks at concrete are also plotted for the same load level to address the plastic hinge length. These plots are given in Fig. 8. Considering the length of yield line of tension bar and concrete cracks, L_p is calculated and normalized with the effective depth of the cross section, d (Table 4).

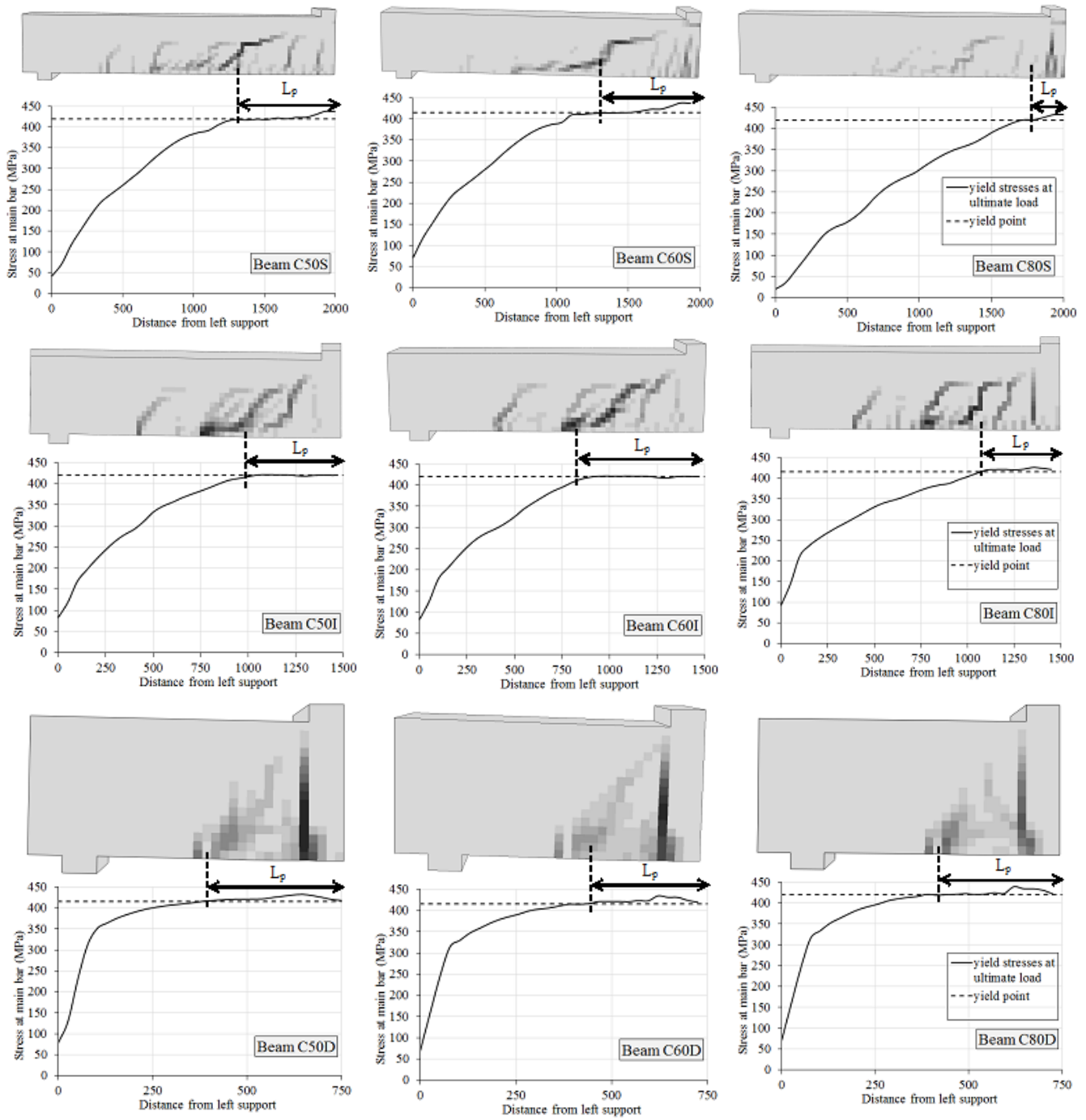


Fig. 8 - Determination of L_p for each parametric beam



Table 4 - Values of L_p for each parametric beam

		Slenderness					
		Deep (D)		Intermediate (I)		Slender (S)	
		L_p (mm)	L_p/d	L_p (mm)	L_p/d	L_p (mm)	L_p/d
Concrete Class	C50	372	0.99	495	1.32	740	1.97
	C60	310	0.83	535	1.43	755	2.01
	C80	303	0.80	481	1.28	357	0.95

For a given steel ratio (presented in Table 3), L_p/d value increases as the slenderness ratio increases. On the other hand, in deep beams, L_p/d value decreases as the concrete class increases. The highest value of L_p/d is obtained as 2.01 for slender beam reinforced with C60 concrete class. The minimum value of L_p/d is obtained as 0.80 for deep beam reinforced with C80 concrete class. L_p/d value is decreased by up to 48% for the biggest concrete class used in this study for slender beams with same shear span. However the decreasing ratio changed 11% and 19% in intermediate and deep beams respectively. On the other hand maximum L_p values are observed when the C60 concrete class were used in intermediate and slender beams. All the deep beams have the least L_p value while the slender beams have the maximum L_p values.

6. Conclusions

Modelling of plastic hinges is quite important since in RC structure analysis dissipation of energy is achieved through these hinges. There are several expressions in literature that defines the location of plastic hinges either by considering yielding of tension steel or contraflexure or both. However, existing experiments in the literature proved that shear span to depth ratio is also very important on the definition of plastic hinge length. In this numerically verified study RC beams with different failure modes are created by considering span to depth ratio. Then plastic hinge length for these beams are determined. Findings are summarized as follows:

- 1) Finite element approach is capable of capturing load-deflection relationship and stresses developed in the steel bar embedded in concrete.
- 2) L_p is correlated with the shear span to depth ratio value which is named as slender, deep and intermediate beam in this study.
- 3) As the reinforced concrete class increases plastic hinge length decreases independent from slenderness.

7. References

- [1] Fenwick RC, Thom CW (1982): Shear deformation in reinforced concrete beams subjected to inelastic cyclic loading. *The University of Auckland Research Report No:279*, Department of Civil Engineering, University of Auckland.
- [2] Corley GW (1966): Rotation capacity of reinforced concrete beams. *ASCE J Struct Div*, vol. 92, 121–146.
- [3] Mattock AH (1967): Discussion of rotational capacity of reinforced concrete beams by W. D. G. Corley. *ASCE J Struct Div*, vol. 93, 519–522.
- [4] Priestley M. J. N. (1987): Park R. Strength and ductility of concrete bridge columns under seismic loading. *ACI Struct J*, vol. 84, 61–76.
- [5] Panagiotakos TB, Fardis MN (2001): Deformations of reinforced concrete members at yielding and ultimate. *ACI Struct J*, vol. 98, 135–48.
- [6] *Federal Emergency Management Agency (2000): FEMA 356 Prestandard and Commentary for the Seismic Rehabilitation of Buildings*. Washington DC.
- [7] Park R, Paulay T (1975): Reinforced Concrete Structures. *John Wiley & Sons*, New York.



- [8] Beeby AW (1997): Ductility in reinforced concrete: why is it needed and how is it achieved. *Structural Engineer*, vol. 75 (18), 311–318.
- [9] Ho J.C.M. (2003): Inelastic design of reinforced concrete beams and limited ductile high-strength concrete columns, *Doctor of Philosophy Dissertation*, The University of Hong Kong, China.
- [10] Berry MP (2006): Performance modeling strategies for modern reinforced concrete bridge columns, *Doctor of Philosophy Dissertation*, University of Washington, USA.
- [11] Bae SJ, Bayrak O (2008): Plastic hinge length of reinforced concrete columns, *ACI Struct J*, vol. 105, 290–300.
- [12] Gu DS, Wu YF, Wu G, Wu ZS (2012): Plastic hinge analysis of FRP confined circular concrete columns, *Construction and Building Materials*, 27(1), 223-233.
- [13] American Concrete Institute (2014): *Building Code Requirements for Structural Concrete*, ACI 318-14, ACI, Detroit, MI.
- [14] Wight JK, Macgregor JG (2012): *Reinforced Concrete Mechanics and Design*, 5th Edition.
- [15] Potisuk T, Higgins CC, Miller TH, and Yim SC (2011): Finite Element Analysis of Reinforced Concrete Beams with Corrosion Subjected to Shear, *Advances in Civil Engineering*, vol. 2011, Article ID 706803, doi:10.1155/2011/706803.
- [16] Agcakoca E, Aktas M (2012): The Impact of the HMCFRP Ratio on the Strengthening of Steel Composite I-Beams, *Mathematical Problems in Engineering*, vol. 2012, Article ID 183906, doi:10.1155/2012/183906.
- [17] Arduini M, Nanni A (1997): Behavior of precracked RC beams strengthened with carbon FRP sheets, ASCE, *Journal of Composites for Construction*, 1 (2), 63–70.
- [18] Coronado AC, Lopez MM (2006): Sensitivity analysis of reinforced concrete beams strengthened with FRP laminates, *Cement and Concrete Composites*, 28 (1), 102-114.
- [19] CEB-FIP MC90 (1993): *Comite Euro-International du Beton*, CEB-FIP Model Code 1990, Bulletin D'Information, No: 215, Lausanne.
- [20] ABAQUS. *Theory Manual*, Version 6.13, Hibbit, Karlsson & Sorensen, Inc., Pawtucket, Rhode Island, USA.
- [21] ABAQUS. *User's Manual*, Version 6.13, Hibbit, Karlsson & Sorensen, Inc., Pawtucket, Rhode Island, USA.
- [22] KAMALI AZ (2012): Shear strength of reinforced concrete beams subjected to blast loading, *Master of Science Thesis*, Stockholm, Sweden.
- [23] Sinha BP, Gerstle KH, Tulin LG (1964): Stress–strain relations for concrete under cyclic loading, *ACI Journal*, vol. 61, 195-211.
- [24] Aktas M, Earls CJ (2006): Minor axis moment-thrust response behavior in steel I-shaped members, *Journal of Structural Engineering-ASCE*, vol. 132, 1079-1086.
- [25] Arduini MDT, Nanni A (1997): Brittle failure in FRP plate and sheet bonded beams, *ACI Structural Journal*, 94 (4), 363-370.
- [26] Sharif A, Al-Sulaimani GJ, Basunbul IA, Baluch MH, Ghaleb BN (1994): Strengthening of initially loaded reinforced concrete beams using FRP plates, *Struct J (ACI)*, 91 (2), no. 2, 160-166.
- [27] Mains RM (1951): Measurement of the distribution of tensile and bond stresses along reinforcing bars, *Journal of the American Concrete Institute*, Proceedings, 48 (3) 225-252.